WWW.IJRPR.COM

International Journal of Research Publication and Reviews

Journal homepage: www.ijrpr.com ISSN 2582-7421

INSILICO STUDIES OF BENZOXAZOLE DERIVATIVES AS ANTICANCER AGENTS AGAINST VEGFR-2

Ms. Ritika [1]*, Prof(Dr.) Nasiruddin Ahmad Farooqui [2] , Mr. Saket [3], Mr. Mohd Salman [4]

[1] Reaseach scholar, Translam institute of pharmaceutical education and research Meerut
[2] Guide, Translam institute of pharmaceutical education and research Meerut
[3] Assistant professor, Royal college of pharmacy wazirpur Gurugram
[4] Assistant professor, Translam institute of pharmaceutical education and research Meerut

ABSTRACT :

The global burden of cancer remains one of the most pressing challenges in modern medicine .In response to the growing problem of drug resistance, advanced in silico drug design methods— *involving the application of structure-guided and ligand-oriented computational techniques.* In this study, the crystallographic structure of VEGFR-2 (PDB ID: 3VHE), complexed with a pyrrolopyrimidine-class inhibitor was utilized to model interactions against the HCT-116 colorectal cancer cell line. A five-point pharmacophore hypothesis was generated, which formed the basis for an atom-based 3D-QSAR model. This model demonstrated strong predictive performance, with a training set correlation coefficient (Q^2 = 0.7536) and a test set regression coefficient (R^2 = 0.8619), confirming its reliability. The top-ranked docked compound was selected for ligand-based virtual screening using the PubChem database. Subsequently, the ten best hits were evaluated through ADME/T analysis. Among the highest ranking ten candidates, the docking scores were observed to vary between –9.116 to –8.635 kcal/mol, outperforming standard references. These candidates were further assessed for their pharmacokinetic and safety profiles. The findings suggest that several benzoxazole derivatives show strong potential as VEGFR-2 inhibitors and could be promising leads for colorectal cancer therapy.

Keywords*:* Benzoxazole, anticancer, molecular docking, pharmacophore, atom-based 3D-QSAR, ADMET.

INTRODUCTION:

Cancer is a multifactorial disease characterized by uncontrolled proliferation of abnormal cells and disruption of normal tissue architecture.(1). Despite widespread use of chemotherapy across nearly all cancer types, drug resistance remains a significant hurdle in treatment success. Various agents known to trigger carcinogenesis include natural toxins, synthetic chemicals, biological substances, and environmental pollutants. While numerous chemotherapeutic agents have been developed, many exhibit considerable side effects and limited efficacy. Consequently, ongoing research aims to discover new anticancer drugs that are potent, safe, cost-effective, and exhibit minimal toxicity.(2)

A hallmark of cancer progression is the evasion of programmed cell death (apoptosis). Defective apoptotic mechanisms are strongly implicated in tumorigenesis, including colorectal cancer. Although Colorectal cancer is recognized as one of the most prevalent malignancies contributing to cancer-related deaths worldwide. By 2030, projections indicate an annual global burden of approximately 2.2 million newly diagnosed cases and around 1.1 million fatalities. (3)

The complexity of its progression, involving uncontrolled cell proliferation, evasion of apoptosis, and angiogenesis, necessitates the discovery of novel therapeutic agents. Among the various mechanisms implicated in tumor development, angiogenesis—mediated primarily by vascular endothelial growth factors (VEGFs)—plays a crucial role in ensuring the tumor's access to nutrients and oxygen. (4)

VEGFR-2, a key receptor tyrosine kinase, mediates most of the angiogenic responses triggered by VEGF-A. Inhibition of VEGFR-2 signaling has shown promising results in controlling tumor growth and metastasis. (5)Consequently, molecules that can block this pathway are of significant interest for anticancer drug development.

Benzoxazole is a heteroaromatic moiety found in many biologically active compounds. Its fusion of a benzene ring with an oxazole structure provides a rigid and pharmacologically favorable framework. Compounds containing this scaffold have shown antimicrobial, anti-inflammatory, antioxidant, and particularly anticancer activity, including inhibition of angiogenesis-related enzymes and kinases.(6)

Computational approaches, including structure- and ligand-based modeling, provide an efficient pathway to evaluate large chemical libraries prior to synthesis. These tools help in predicting biological activity, target binding, and pharmacokinetic

2.0 Aim and Objective

2.1 Aim

To conduct in silico evaluation of benzoxazole-based analogs for their potential as inhibitors of the VEGFR-2 kinase involved in tumor angiogenesis.

2.2 Objectives

- To retrieve and utilize the crystallographic structure of VEGFR-2 (PDB ID: 3VHE), complexed with a pyrrolopyrimidine-class inhibitor, for molecular modeling studies.
- To build a *compound dataset* of benzoxazole-based molecules with reported anticancer activity, collected from published literature and the *PubChem* database.
- To conduct *molecular docking* simulations of the selected benzoxazole derivatives using *Maestro (Schrödinger v13.6)* to analyze binding interactions with VEGFR-2.
- To generate Pharmacophore hypothesis generated from active ligands using structural alignment tools, enabling the extraction of essential molecular features contributing to activity.
- To develop a three dimensional-QSAR model using atom-based spatial descriptors derived from the selected pharmacophore, with statistical validation of the predictive model.
- To execute *ligand-based virtual screening* using the pharmacophore model to identify structurally similar hits from the filtered PubChem database.
- To perform *ADME/T predictions* for the top-ranked docked compounds using *ADMET Lab 2.0*, evaluating their drug-likeness, safety, and toxicity profiles.
- To prioritize benzoxazole compounds with promising docking scores, favorable pharmacokinetics, and low toxicity as potential *VEGFR-2 inhibitors* for further preclinical research.

3.0 Material and method

This chapter outlines the digital tools and computational approaches employed in the study. It includes a detailed description of the software, datasets, and methodologies used for ligand-derived models and target structure-based design strategies targeting VEGFR-2..

3.1 Software Tools and Online Platforms

All computational modeling and simulations—such as pharmacophore generation, 3D-QSAR development, molecular docking, and virtual screening—were executed using *Schrödinger Suite (Maestro v13.6, 2022, LLC, NY)***.** Additionally, freely available platforms like *PubChem* and *ADMETlab 2.0* were used for compound sourcing and in silico pharmacokinetic evaluation. (7)

3.2 Methodological Framework

3.2 Methods

3.2.1 Ligand-based drug design

3.2.1.1 Compound Dataset

A total of *93 benzoxazole derivatives* with reported *IC_{50} values* against the *HCT-116 colon carcinoma line* were curated from scientific literature published post-2015. The IC_{50} values ranged from *4.011 μM to 5.554 μM***,** and were converted to *pIC_{50}* format ($-\log_{10}IC_{50}$) for use in pharmacophore and QSAR modeling.(8)

4.2.1.2 Protein Structure Retrieval- crystallographic structure of VEGFR-2 (PDB ID: 3VHE), complexed with a pyrrolopyrimidine-class inhibitor, for molecular modeling studies.

The three dimensional *structure of VEGFR-2* complexed with a pyrrolopyrimidine-based inhibitor (PDB ID: *3VHE*, resolution 1.55 Å) (9) Retrieved from the Protein PDB repository. The ligand present in the complex was *1-{2-fluoro-4-[(5-methyl-5H-pyrrolo[3,2-d]pyrimidin-4-yl)oxy]phenyl}-[3-(trifluoromethyl)phenyl]urea***.** Structural integrity and geometry were evaluated using a *Ramachandran plot***,** which indicates favored and allowed conformational regions.

3.2.1.3 preparation of protein

The target protein was refined through the Protein Preparation Wizard integrated within the Maestro suite. Initial preprocessing involved the deletion of

water molecules, heteroatoms, and additional non-essential chains. Hydrogen atoms were added to ensure structural stability, and incomplete regions such as loops and side chains were modeled appropriately. The resulting structure underwent energy minimization using the OPLS-2005 force field to achieve an optimized conformation. A receptor grid encompassing the active site was then created using Glide, setting the stage for docking studies. (10,11)

3.2.1.4 Ligand Preparation

All 93 compounds were initially drawn in 2D using *ChemDraw v16* and then converted to 3D. Protonation were set at *pH 7.4***,** and no conformers were generated beyond the default. To optimize the geometry, energy minimization was applied with the OPLS-2005 force field protocol. (12)

Table 3.2.1: Library of benzoxazole derivatives with IC50 values (µM)

S.no.	Compounds	Chemical Structures	IC50 (µM) HCT 116	pIC50 (µM)
1	AS1	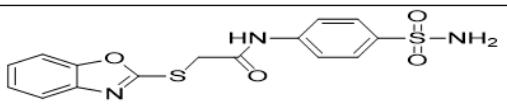	4.3152	5.365
2	AS2	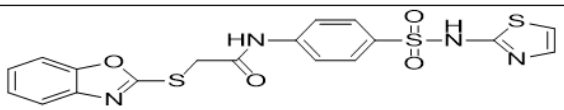	4.7650	5.322
3	AS3	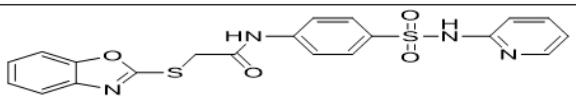	4.7857	5.320
4	AS4	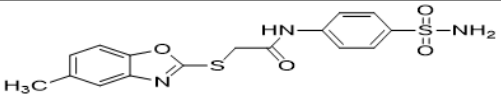	4.5955	5.338
5	AS5	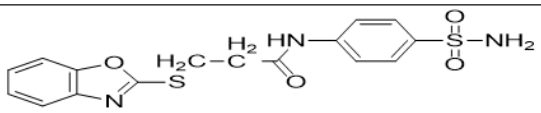	4.2019	5.377
6	AS6	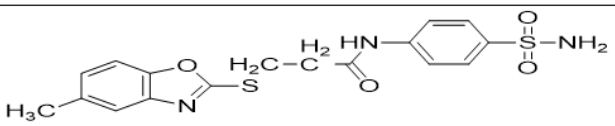	4.5782	5.339
7	AS7	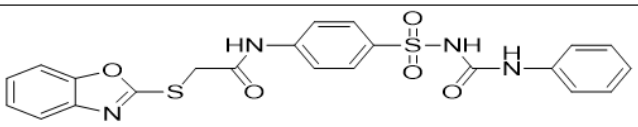	4.6828	5.329
8	AS8	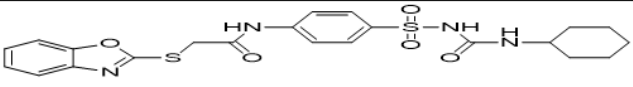	4.7368	5.325
9	AS9	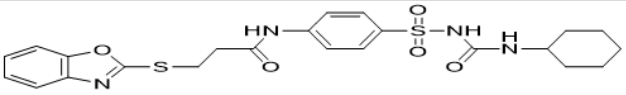	5.1463	5.289
10	AS10	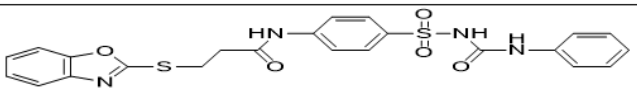	5.0214	5.299

11	AS11	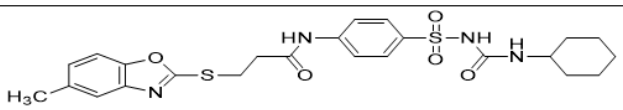	5.1593	5.287
12	AS12	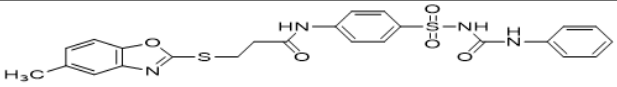	5.0410	5.297
13	AS13	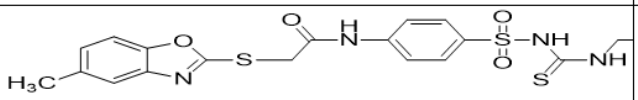	4.5319	5.344
14	AS14	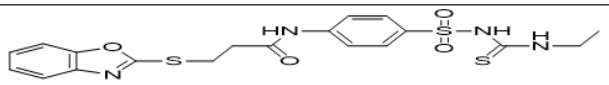	5.1018	5.292
15	AS15	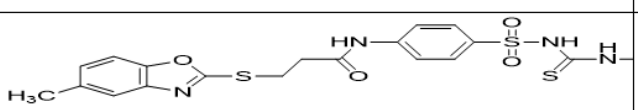	4.9038	5.309
16	AS16	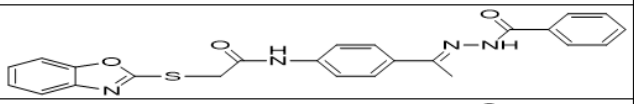	4.5018	5.347
17	AS17	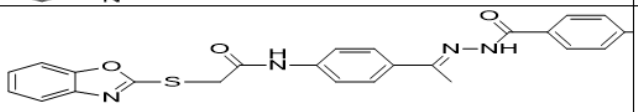	4.5158	5.345
18	AS18	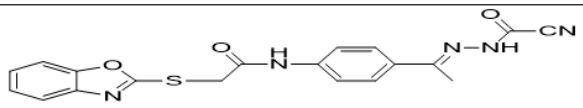	4.1880	5.378
19	AS19	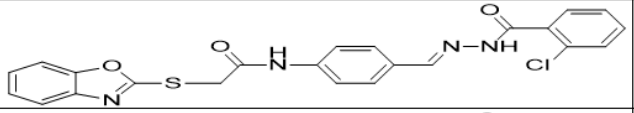	4.1230	5.385
20	AS20	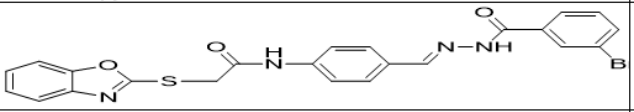	4.1066	5.387
21	AS21	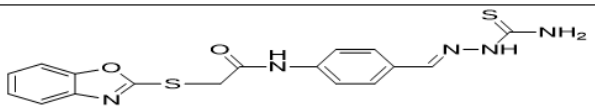	4.3458	5.362
22	AS22	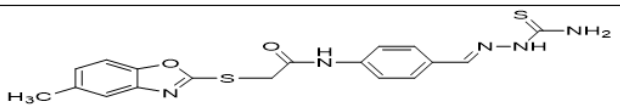	4.9851	5.302
23	AS23	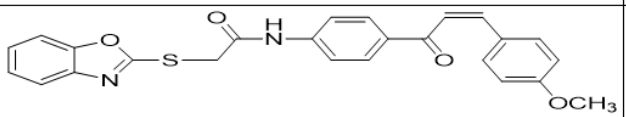	4.3429	5.362
24	AS24	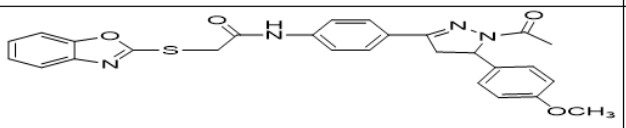	4.3536	5.361
25	AS25	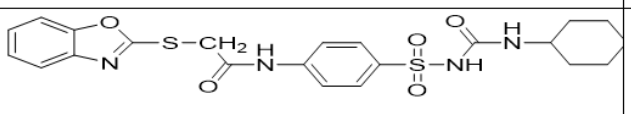	18.33	4.737
26	AS26	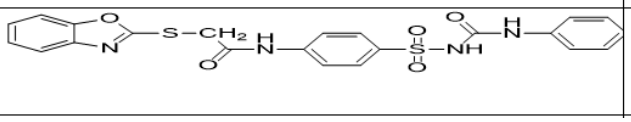	20.76	4.683

27	AS27	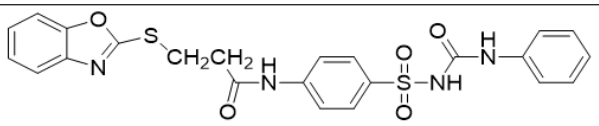	9.52	5.021
28	AD28	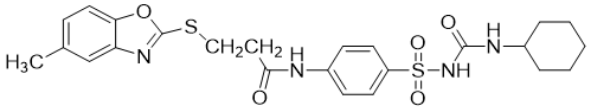	6.93	5.159
29	AS29	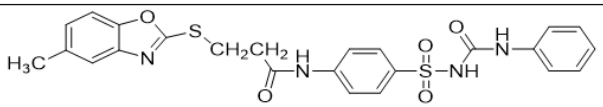	9.10	5.041
30	AS30	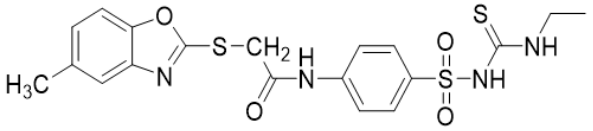	29.38	4.532
31	AS31	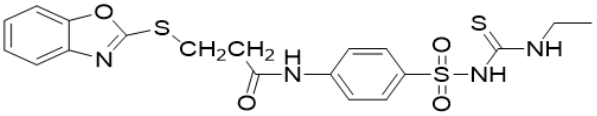	7.91	5.102
32	AS32	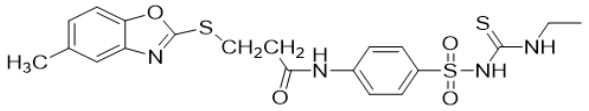	12.48	4.904

33	AS33	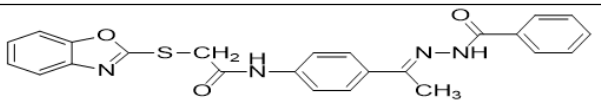	31.49	4.502
34	AS34	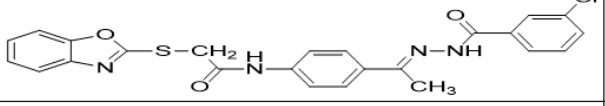	75.33	4.123
35	AS35	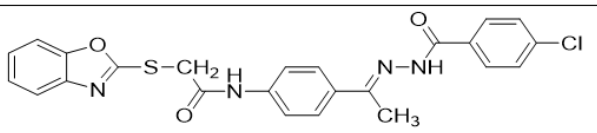	30.49	4.516
36	AS36	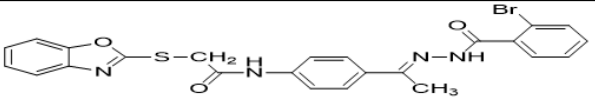	78.24	4.107
37	AS37	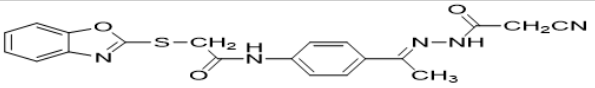	64.86	4.188
38	AS38	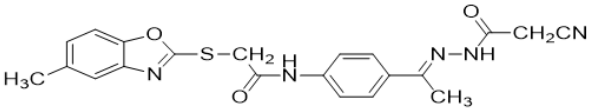	46.10	4.336
39	AS39	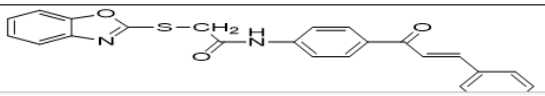	45.4	4.343

40	AS40	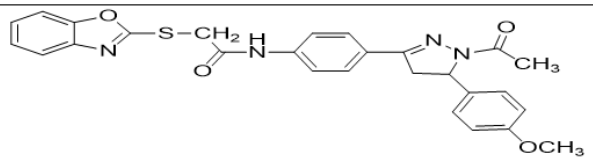	44.3	4.354
41	AS41	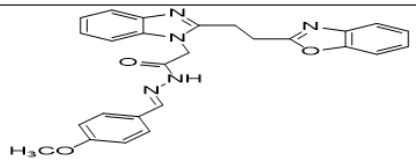	84.8	4.072
42	AS42	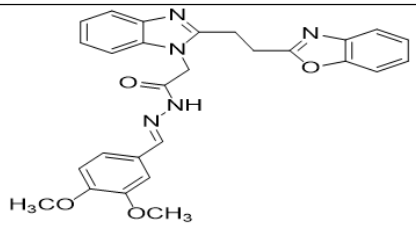	39.9	4.399
43	AS43	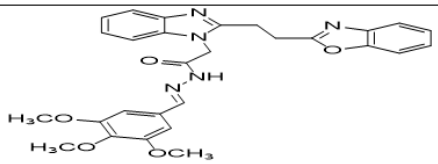	24.5	4.611
44	AS44	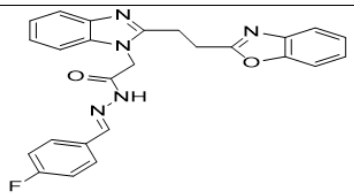	78.3	4.106
45	AS45	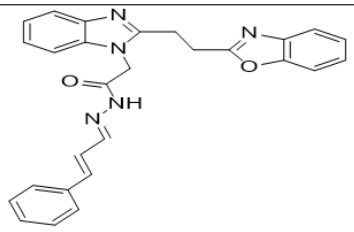	70.6	4.151
46	AS46	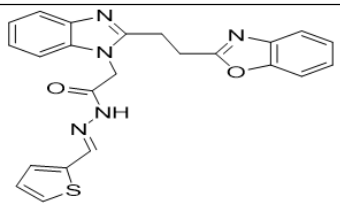	96.1	4.017
47	AS47	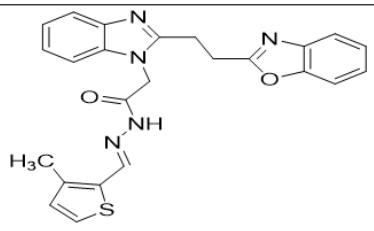	45.5	4.342
48	AS48	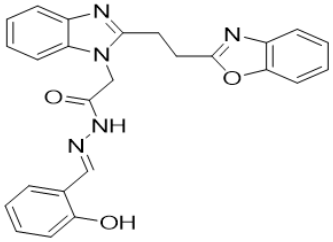	35.6	4.449

49	AS49	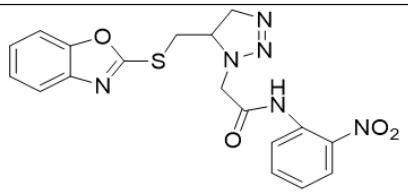	97.5	4.011
50	AS50	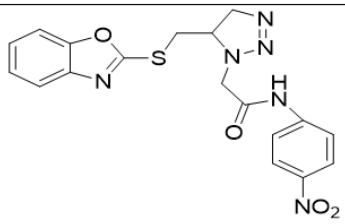	73.1	4.136
51	AS51	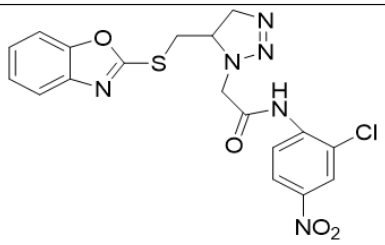	22.5	4.648
52	AS52	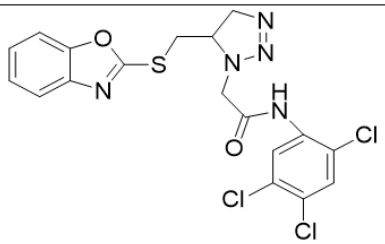	85.3	4.069
53	AS53	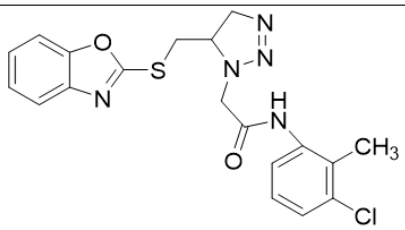	84.6	4.073
54	AS54	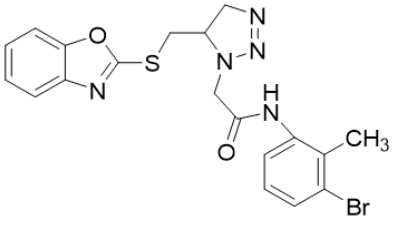	72	4.143
55	AS55	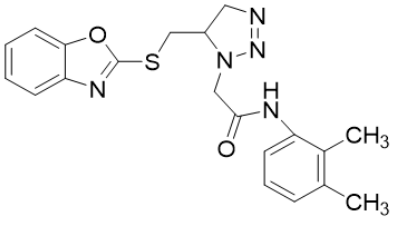	66.1	4.180
56	AS56	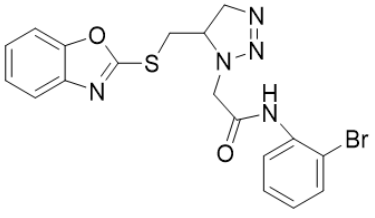	90	4.046

57	AS57	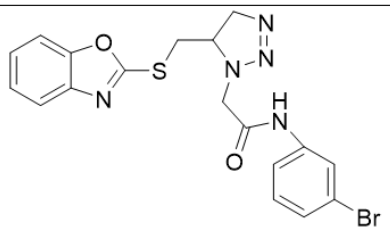	38.3	4.417
58	AS58	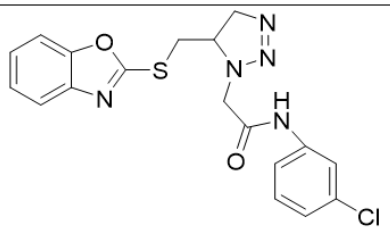	50	4.301
59	AS59	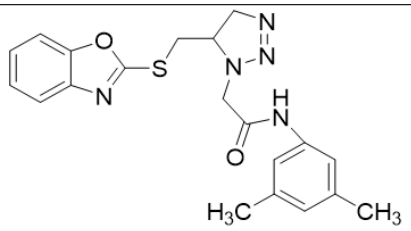	40.7	4.390
60	AS60	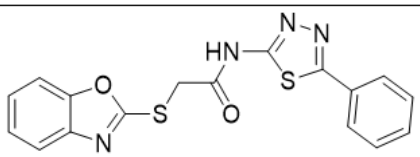	12.45	4.905
61	AS61	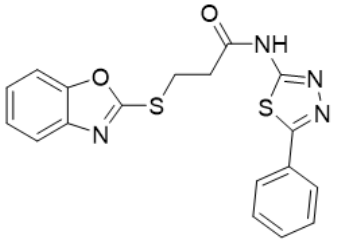	6.99	5.156
62	AS62	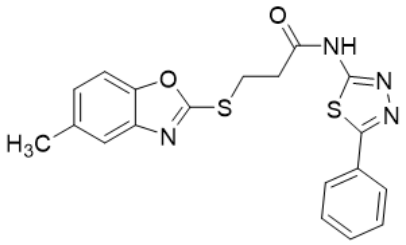	5.76	5.240
63	AS63	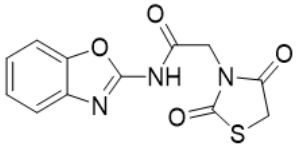	32.77	4.485

64	AS64	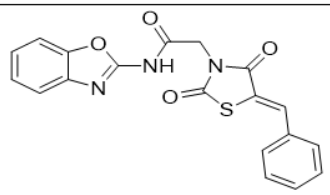	25.59	4.592
65	AS65	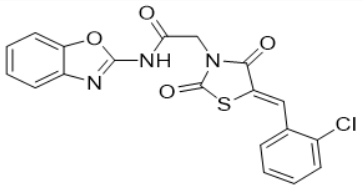	15.43	4.812
66	AS66	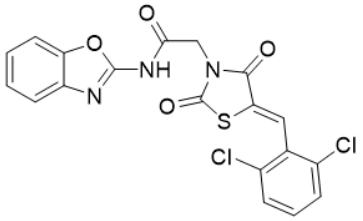	21.12	4.675
67	AS67	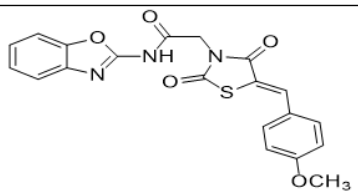	11.16	4.952
68	AS68	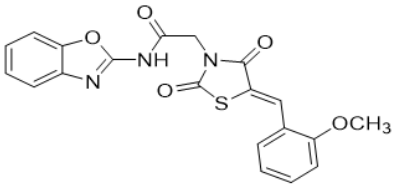	24.77	4.606
69	AS69	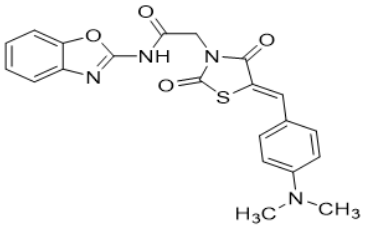	22.11	4.655
70	AS70	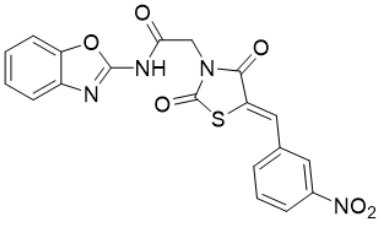	24.87	4.604
71	AS71	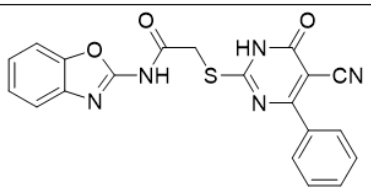	22.66	4.645
72	AS72	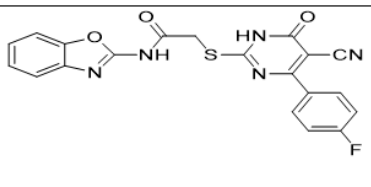	23.66	4.626

73	AS73	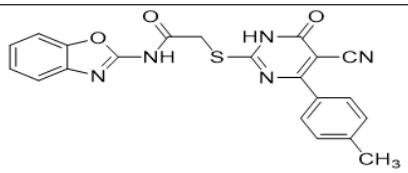	12.14	4.916
74	AS74	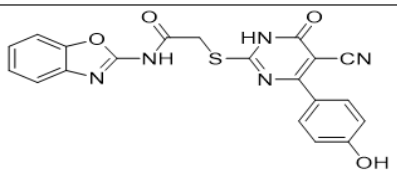	23.89	4.622
75	AS75	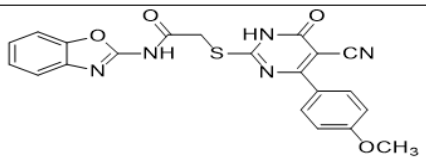	16.22	4.790
76	AS76	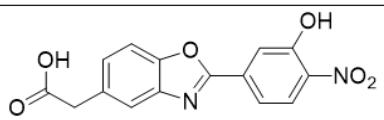	41.95	4.377
77	AS77	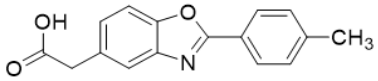	15.02	4.823
78	AS78	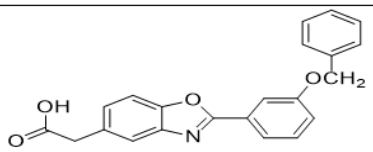	84.54	4.073
79	AS79	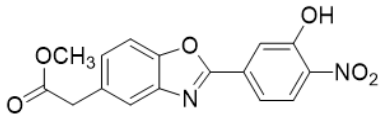	58.35	4.234
80	AS80	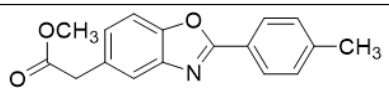	20	4.699
81	AS81	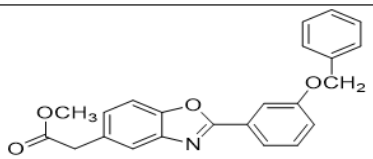	40.03	4.398
82	AS82	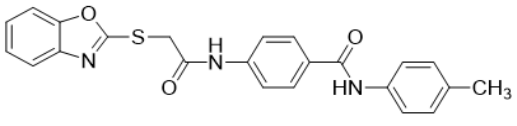	10.06	4.997
83	AS83	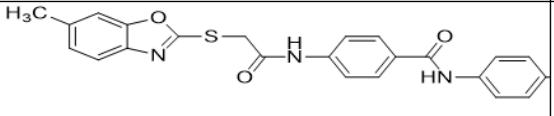	11.57	4.937

84	AS84	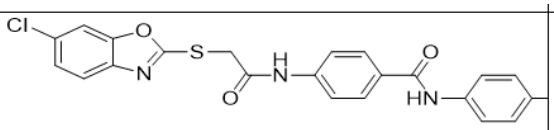	6.12	5.213
85	AS85	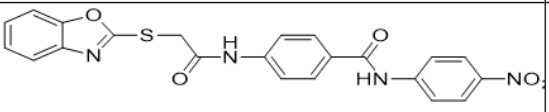	2.79	5.554
86	AS86	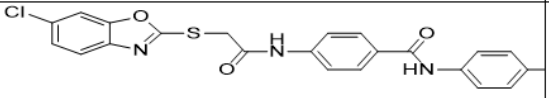	3.29	5.483
87	AS87	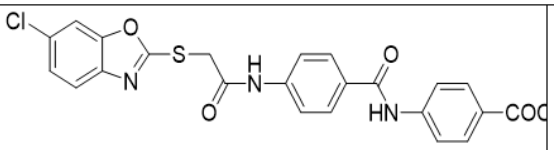	10.36	4.985
88	AS88	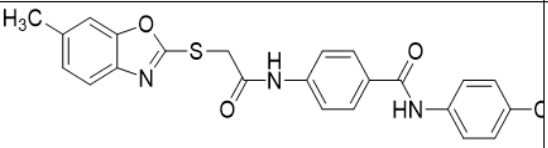	2.94	5.532
89	AS89	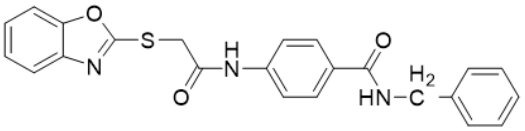	8.53	5.069
90	AS90	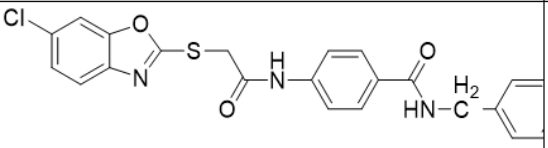	18.23	4.739
91	AS91	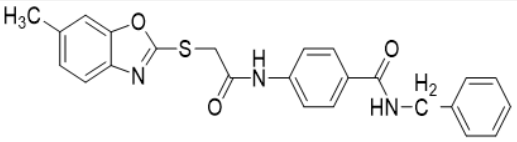	8.09	5.092
92	AS92	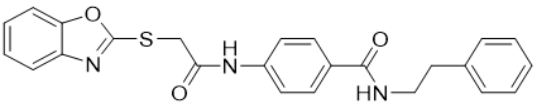	14.16	4.849
93	AS93	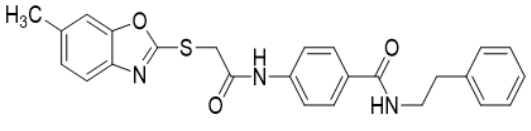	16.36	4.786

3.2.1.5 A Pharmacophore model generation

In this phase of the study, a pharmacophore model was constructed using a ligand-based strategy to identify key interaction features essential for VEGFR-2 inhibition. The model was built using tools from the Schrödinger Maestro platform, which facilitates molecular alignment, hypothesis development, and QSAR modeling workflows. A total of 93 benzoxazole-based compounds were prepared and conformationally optimized. For each compound, multiple conformers (up to 50) were generated to account for structural flexibility. Molecules were categorized as active ($pIC_{50} \geq 5$) or inactive ($pIC_{50} < 5$) based on reported bioactivity.(13)

Pharmacophoric hypotheses were derived from six key molecular features: hydrophobic centers (H), H-bond donors (D), H- bond acceptors (A), aromatic rings (R), and both positively (P) and negatively charged groups (N).From the dataset, 43 active and 57 inactive compounds were selected to build a series of pharmacophore hypotheses, each accommodating a maximum of five feature types. (14) These hypotheses were evaluated using scoring functions such as site score, vector alignment, volume match, and overall survival score.

Among all models, the one designated as AAHRR_1—comprising two acceptor features, one hydrophobic center, and two aromatic rings—demonstrated the best predictive capacity and was chosen for further validation. External validation was conducted using a decoy set obtained from the DUD-E (Database of Useful Decoys: Enhanced), including 109 decoys and 42 known VEGFR-2 actives, creating a test set of 151 molecules. The AAHRR_1 model was assessed based on several key metrics including: Following validation, the *AAHRR_1 pharmacophore hypothesis* was used as a template for developing a *3D-QSAR model* in the next stage of this study. (15)

Table 3.2.2: All 11 generated hypothesis by PHASE module and their parametric scores.

Hypothesis	Survival Score	Site Score	Vector Score	Volume Score
AAHRR_1	5.692	0.8026	0.972	0.644
HRRR_1	5.517	0.8176	0.959	0.626
HRRR_2	5.388	0.7988	0.940	0.562
AHRR_1	5.376	0.8009	0.964	0.641
AHRR_2	5.312	0.7437	0.940	0.633
AHRR_3	5.291	0.7451	0.936	0.614
AAHR_1	5.274	0.9751	0.998	0.567
AARR_1	5.200	0.8441	0.962	0.611
AHRR_4	5.191	0.7307	0.936	0.545
AARR_2	5.16	0.7856	0.970	0.641
AAHR_2	5.133	0.7643	0.951	0.606

3.2.1.6 3D-QSAR Model Construction

To further explore the structure-activity relationship of benzoxazole derivatives, a three-dimensional quantitative structure-activity relationship (3D-QSAR) model was built using the atom-based QSAR method. This study utilized the *PHASE module* from *Schrödinger (Maestro v13.6)* to construct the model using the most predictive pharmacophore hypothesis, *AAHRR_1*. **(16)**

Out of the 93 compounds, 70% were assigned to the training set, while the remaining 30% formed the test set. The full dataset comprising *93 ligands* was randomly split into two subsets: *70 compounds (≈75%) for training*, and *23 compounds (≈25%) for testing* the model's robustness (Table 4.2.3).The model was developed using Partial Least Squares (PLS) regression with a maximum of five components. A spatial grid of 1 Å was applied to map molecular fields around aligned ligands. (17)

For model internal validation, leave-one-out (LOO) cross-validation was applied. Descriptors used included electrostatic, steric, hydrophobic, hydrogen bonding, and ionizable properties. The model effectively captured variations in biological activity across structurally diverse ligands.

Contour maps were generated to interpret the spatial effects of individual substituents on potency. These visualizations helped pinpoint regions where certain functional groups could improve or diminish inhibitory potential.

Table 3.2.3: Dataset of 3D-QSAR model built by AAHRR_1 hypothesis with their docking score, observed and predicted activity (pIC_{50}).

Compound no.	QSAR set	Observed activity	Predicted activity
AS1	Test	5.365	5.022
AS2	Training	5.322	5.330

AS3	Training	5.320	5.381
AS4	Test	5.338	4.934
AS5	Training	5.377	5.475
AS6	Training	5.339	5.412
AS7	Training	5.329	5.032
AS8	Test	5.325	5.082
AS9	Training	5.289	5.243
AS10	Training	5.299	5.209
AS11	Training	5.287	5.276
AS12	Training	5.297	5.345
AS13	Training	5.344	5.199
AS14	Test	5.292	5.083
AS15	Test	5.309	5.037
AS16	Training	5.347	5.897
AS17	Training	5.345	4.995
AS18	Training	5.378	5.102
AS19	Training	5.385	5.269
AS20	Training	5.387	5.212
AS21	Training	5.362	5.339
AS22	Training	5.302	5.285
AS23	Training	5.362	5.260
AS24	Training	5.361	4.813
AS25	Test	4.737	5.082
AS26	Training	4.683	5.021
AS27	Training	5.021	5.039
AS28	Training	5.159	5.164
AS29	Training	5.041	5.086
AS30	Training	4.532	4.466

AS31	Test	5.102	5.019
AS32	Training	4.904	4.874
AS33	Training	4.502	4.897
AS34	Training	4.123	4.489
AS35	Training	4.516	4.952
AS36	Training	4.107	4.447
AS37	Training	4.188	4.296
AS38	Training	4.336	4.115
AS39	Test	4.343	4.772
AS40	Training	4.354	4.813
AS41	Test	4.072	4.139
AS42	Training	4.399	4.474
AS43	Test	4.611	4.492
AS44	Test	4.106	4.276
AS45	Training	4.151	4.114
AS46	Training	4.017	3.976
AS47	Training	4.342	4.329
AS48	Training	4.449	4.503
AS49	Training	4.011	3.963
AS50	Training	4.136	4.103
AS51	Training	4.648	4.698
AS52	Training	4.069	3.998
AS53	Training	4.073	4.059
AS54	Training	4.143	4.056
AS55	Test	4.180	4.188
AS56	Training	4.046	3.995
AS57	Test	4.417	4.474
AS58	Training	4.301	4.263
AS59	Test	4.390	4.369
AS60	Training	4.905	4.988
AS61	Training	5.516	5.150
AS62	Test	5.240	5.054

AS63	Training	4.485	4.489
AS64	Test	4.592	4.686
AS65	Training	4.812	4.764
AS66	Training	4.675	4.751
AS67	Training	4.952	4.871
AS68	Training	4.606	4.585
AS69	Training	4.655	4.741
AS70	Training	4.604	4.704
AS71	Test	4.645	4.641
AS72	Training	4.626	4.810
AS73	Training	4.916	4.908
AS74	Training	4.622	4.625
AS75	Test	4.790	4.978
AS76	Training	4.377	4.411
AS77	Training	4.823	4.778
AS78	Training	4.073	4.075
AS79	Test	4.234	4.416
AS80	Training	4.699	4.792
AS81	Training	4.398	4.312
AS82	Training	4.997	5.071
AS83	Training	4937	4.910
AS84	Training	5.213	5.184
AS85	Test	5.554	5.239
AS86	Training	5.483	5.356
AS87	Test	4.985	4.874
AS88	Training	5.532	5.502
AS89	Test	5.069	4.774
AS90	Training	4.739	4.818
AS91	Training	5.092	5.282
AS92	Test	4.849	5.017
AS93	Training	4.786	4.712

3.2.1.7 Virtual screening guided by molecular docking

Structure-based virtual screening was conducted using molecular docking to identify potent VEGFR-2 binders.. In this study, the *PubChem chemical database* was used to identify compounds structurally similar to reference benzoxazole compound was used as a query for similarity search within the PubChem database, yielding 595 structurally related molecules. From this search, *595 structurally related hits* were retrieved and processed. The 2D structures were prepared using LigPrep and docked into the VEGFR-2 binding site using the Glide XP docking protocol. Glide scores were calculated for each ligand, and top-ranked molecules were shortlisted for further study. (18)

Following docking, the top *five compounds* with the most favorable docking scores and binding interactions were shortlisted. These selected ligands were then subjected to *ADME and toxicity evaluations* to determine their pharmacokinetic profiles and potential safety for further drug development..(19)

3.2.1.8 *In silico* ADME screening and toxicity predictions

To evaluate the *drug-likeness, safety, and pharmacokinetic behavior* of the shortlisted ligands, an in silico *ADME/T analysis* was carried out using the *ADMETlab 2.0* online platform. This evaluation included core pharmacokinetic properties—namely *Absorption, Distribution, Metabolism, Excretion (ADME)*—alongside *toxicity assessments* to better understand the systemic behavior of each compound. (20)

Key pharmacokinetic parameters included absorption efficiency, blood-brain barrier penetration, CYP450 enzyme interactions, and systemic clearance.were considered. These descriptors help predict whether a molecule will exhibit acceptable bioavailability and metabolic stability.

To assess *toxicity*, the selected five compounds were screened for parameters such as *hepatotoxicity*, *mutagenicity (AMES test)*, *carcinogenic potential*, *immunotoxicity*, and *cardiac toxicity* (via *hERG inhibition*). These qualitative and quantitative endpoints provided crucial insights into the *risk profile* of each candidate molecule. (20)

The analysis revealed that all five compounds satisfied *Lipinski's Rule of Five*, suggesting good oral bioavailability. Other parameters like *log P (partition coefficient)*, *Caco-2 permeability*, *volume of distribution (VD)*, and *plasma protein binding (PPB)* were also within acceptable limits. Compounds with lower *CYP inhibition* and minimal predicted *toxic side effects* were considered the most promising for further development.

In conclusion, this computational pharmacokinetic profiling provided a comprehensive understanding of how each lead compound may behave in vivo, supporting their potential as *VEGFR-2 inhibitors* in cancer therapy.(21)

4.0 Results and Discussion

4.1 Ligand-based drug design

4.1.1 Pharmacophore hypothesis analysis

Out of the eleven hypotheses generated during ligand alignment, the *five-point AAHRR_1* hypothesis was selected as the most efficient based on its statistical performance: survival score (5.693), strong vector match (0.972), volume alignment (0.644), and site score (0.8026). This model was subsequently validated using a decoy set from the *DUD-E database*, which included *119 decoys and 1 known active compound*.

The validated pharmacophore model yielded strong discrimination metrics, such as an *Enrichment Factor (EF1%) of 100.15*, *AUAC of 1.00*, *BEDROC (160.9) value of 1.0*, **and** *ROC value of 1.00*. The corresponding *ROC curve* displayed a sharp upward slope toward the top-left corner, suggesting excellent ranking of active over inactive compounds. This indicates high reliability of the model.

According to Figure 5.1.2, the AAHRR_1 pharmacophore hypothesis highlights that two H-bond acceptor features, a single hydrophobic interaction site, and two aromatic moieties are essential for VEGFR-2 suppression.

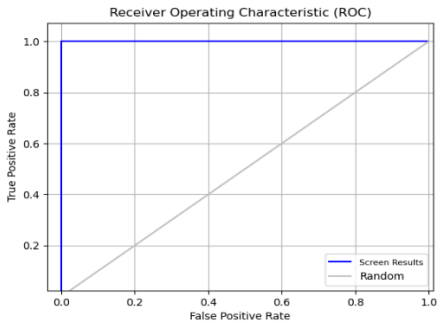

Figure 4.1.1: A ROC plot of the best generated hypothesis AHHRR- 1

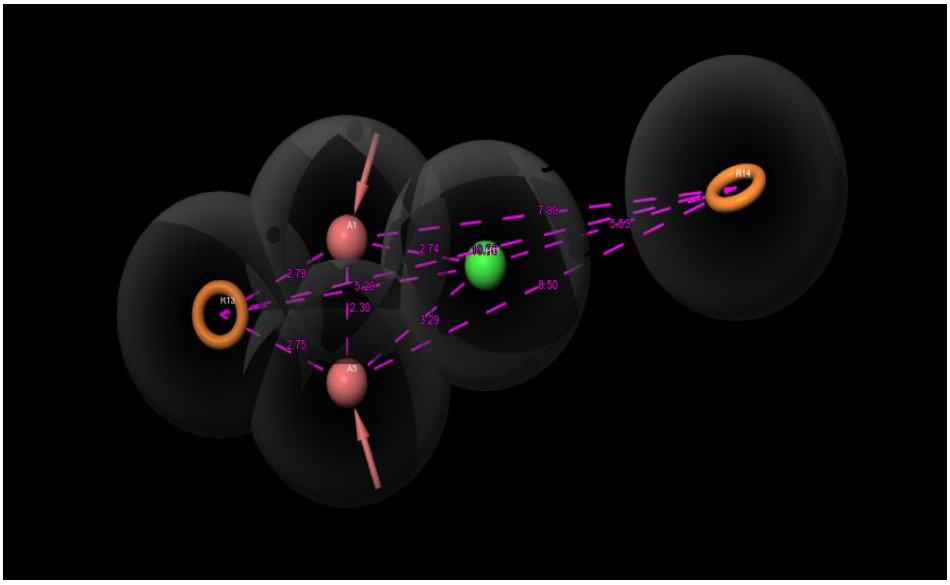

Figure 4.1.2: A five point generated pharmacophore model (AAHRR_1) by PHASE module.

4.1.2 ***3D-QSAR Model Validation***

To confirm the stability and reliability of the atom-based 3D-QSAR model built on AAHHR_1, LOO cross-validation was performed. The model utilized a five-component PLS regression. The model demonstrated strong statistical reliability with the following results: $Q^2 = 0.7536$, $R^2 = 0.8619$, F = 79.9, P = 3.53e−26, SD = 0.1819, and RMSE = 0.22. These metrics confirm the internal predictive power and accuracy of the model.

Scatter plots of the training and test sets confirmed that most compounds clustered closely around the regression line, indicating that the model predicted activities that were consistent with observed results. The regression equation for the test set was **y =** 0.63x + 1.72, with $R^2 = 0.79$, showing reliable external validation as well.(Figure 5.1.3).

Table 4.1.1:PLS parameters for 3D-QSAR model (AAHRR_1)

PLS Factor	SD	R^2	F	P	Stability	Q^2	RMSE	Pearson-R
1.	0.3405	0.4858	64.2	2.06e-11	0.952	0.5881	0.29	0.7800
2.	0.2958	0.6176	54.1	1.03e-14	0.878	0.6694	0.26	0.8322
3.	0.2363	0.7597	69.5	2.12e-20	0.62	0.7250	0.24	0.8604
4.	0.2080	0.8166	72.4	3.15e-23	0.481	0.7769	0.21	0.8973
5.	0.1819	0.8619	79.9	3.53e-26	0.361	0.7536	0.22	0.8900

Table 4.1.2: Statistical data of Atom based 3D-QSAR (AAHRR_1)

PLS Factors	HBD	Hydrophobic/ non-polar	Negative ionic	Positive ionic	Electron – withdrawing
1	0.041726	0.592860	0.008467	0.009740	0.263628
2	0.045626	0.579252	0.009068	0.010450	0.267664
3	0.049485	0.578754	0.011390	0.012782	0.264609
4	0.052130	0.571006	0.012490	0.013934	0.263545
5	0.054173	0.571766	0.013353	0.014966	0.258093

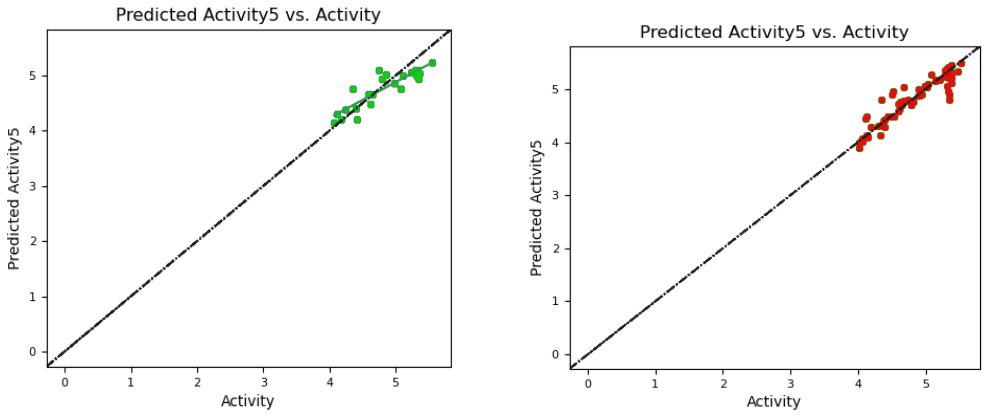

(a) **(b)**

Figure 4.1.3 presents a plot comparing actual biological activity (X-axis) with the predicted values (Y-axis) for compounds in both the test (a) and training (b) sets derived from the AAHRR_1 hypothesis. The regression line for the test set follows the equation $y = 0.63x + 1.72$, with a correlation coefficient (R^2) of 0.79.

4.1.3 Contour Map Computation

The contour map analysis under the atom-based 3D-QSAR approach helps elucidate how specific molecular features influence biological activity. These spatial maps provide a visual representation of favorable and unfavorable interactions associated with molecular moieties.

For the *hydrogen bond donor (HBD)* feature (Figure 5.1.4(1a)), the most active compound, AS91, displayed blue-shaded areas around the amide groups adjacent to the benzoxazole ring. These regions indicate enhanced binding potential due to favorable donor characteristics. In contrast, compound AS50 showed red zones in similar locations (Figure 5.1.4(1b)), reflecting poor contribution to activity and suggesting the need for structural improvements.

In the *hydrophobic contour map* (Figure 5.1.4(2a)), AS91 again exhibited prominent blue cubes near its benzene and acetamide segments, underlining their significance in mediating anticancer effects. Meanwhile, red contours near the sulfur and terminal nitrobenzene suggest these parts may benefit from alteration. The least active compound AS50 showed largely red areas across its structure (Figure 5.1.4(2b)), implying a reduction in hydrophobic compatibility and potential activity.

Lastly, the *electron-withdrawing property* (Figure 5.1.4(3a)) of AS91 revealed blue regions around the acetamide and terminal nitro groups, indicating enhanced receptor interaction. A red region near the hydrogen in the amide group hints at a site with reduced efficiency. In AS50, strong red zones in the 1,2,3-triazole ring and nitrobenzene denote poor interaction, contributing to weak biological effects (Figure 5.1.4(3b)).

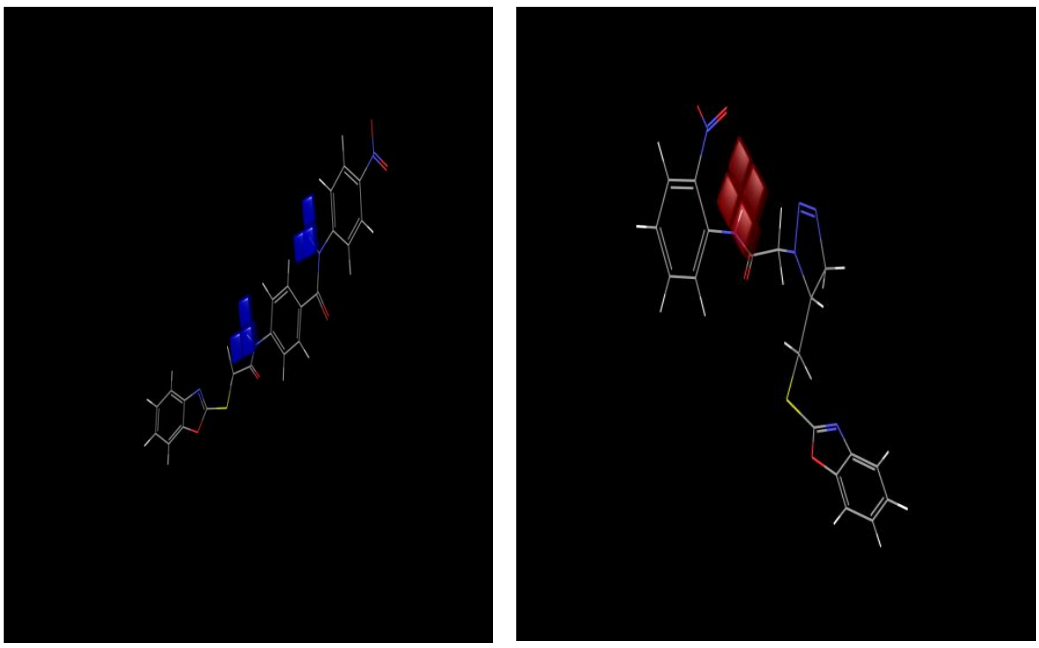

1(a) **1 (b)**

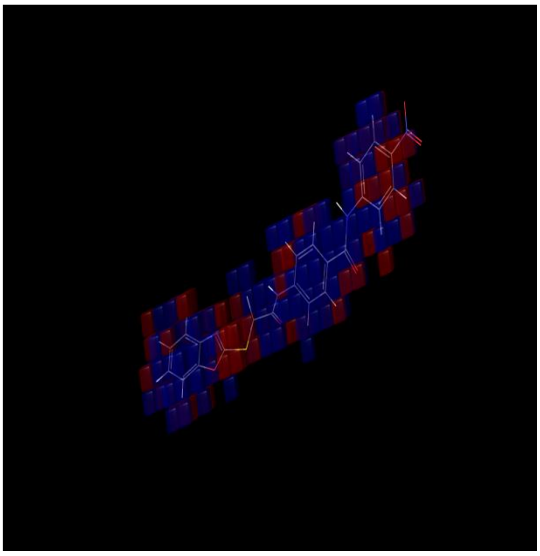

2(a)

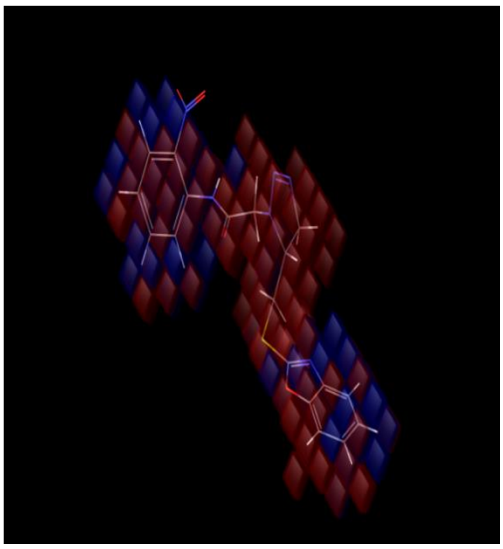

2 (b)

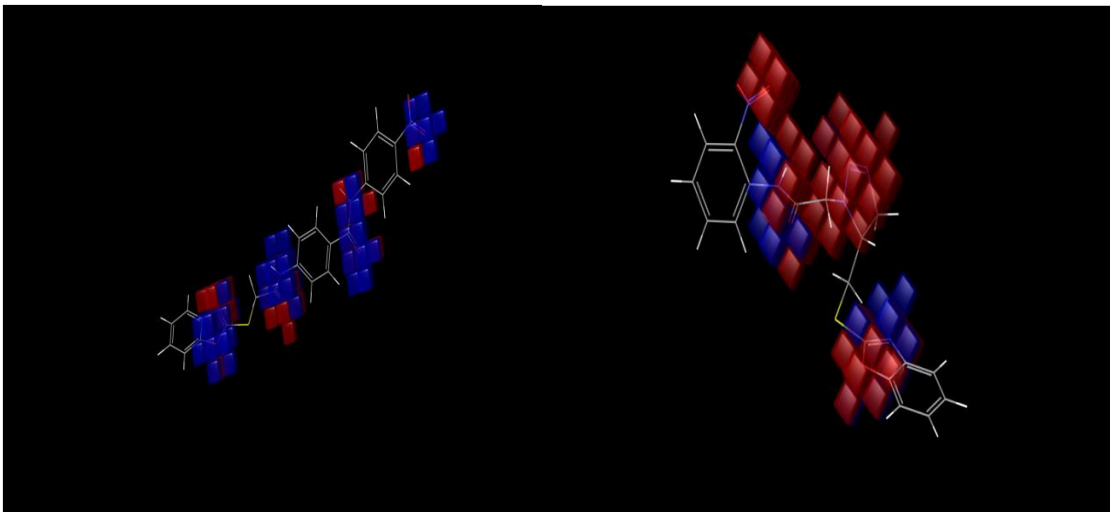

3(a) **3 (b)**

Figure 4.1.4 depicts the spatial distribution of molecular features derived from the 3D-QSAR analysis of compound AS91 (highly active) and AS50 (least active). The subfigures for AS91—(1a) H-bond donor, (2a) hydrophobic zones, and (3a) electron-withdrawing regions—contrast with AS50's corresponding maps in (1b), (2b), and (3b). The contour plots use blue regions to denote areas where specific molecular properties contribute positively to VEGFR-2 inhibition, while red regions signal unfavorable influence on biological activity..

4.1.4 Molecular docking

Docking analyses were performed to investigate how effectively benzoxazole derivatives interact with the VEGFR-2 protein**,** and the outcomes were compared to a known anticancer reference drug, *Floxuridine*. Among the docked molecules, the top-performing ligand was further explored for structural similarity using the *PubChem* chemical database. (22) This similarity search led to the identification of *119 analogs***,** which were later subjected to XP docking using the Glide software. (23)

From this screening, the compound *CID 170501037* The compound exhibited a docking energy of −9.116 kcal/mol, demonstrating stronger binding affinity than Floxuridine, which recorded an energy value of −7.865 kcal/mol (refer to Table 5.1.3). This lead compound exhibited a strong hydrogen bonding interaction with the *CYS919* residue, suggesting a superior fit and binding strength compared to the reference standard. Due to its strong interaction profile and high binding affinity, *CID 170501037* was marked as the *most promising candidate* among all the screened ligands.

Additionally, the *top five ligands* were analyzed in terms of their interaction profiles, including amino acid residues involved and their glide energy scores (see Table 5.1.4). These interactions further validated the docking accuracy and highlighted the potential of the screened compounds as *VEGFR-2 inhibitors***.**

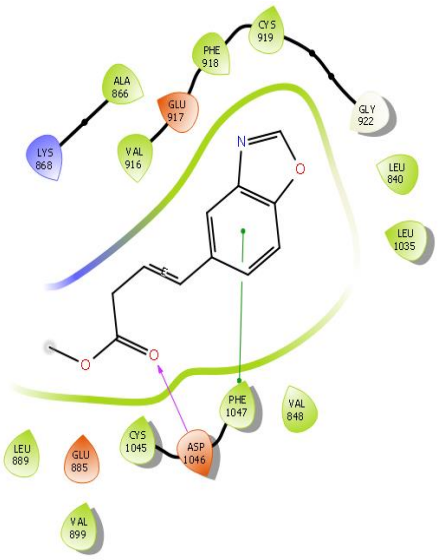
CYS 919
PHE 918
ALA 866
GLU 917
GLY 922
LYS 868
VAL 916
LEU 840
LEU 1035
PHE 1047
VAL 848
CYS 1045
ASP 1046
LEU 889
GLU 885
VAL 899

1(a)

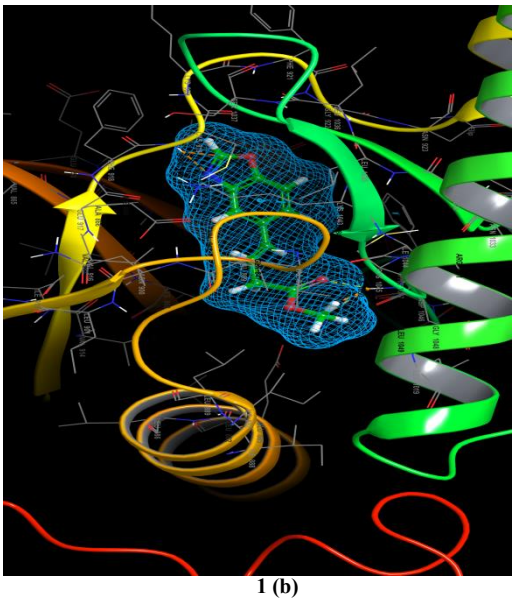

1 (b)

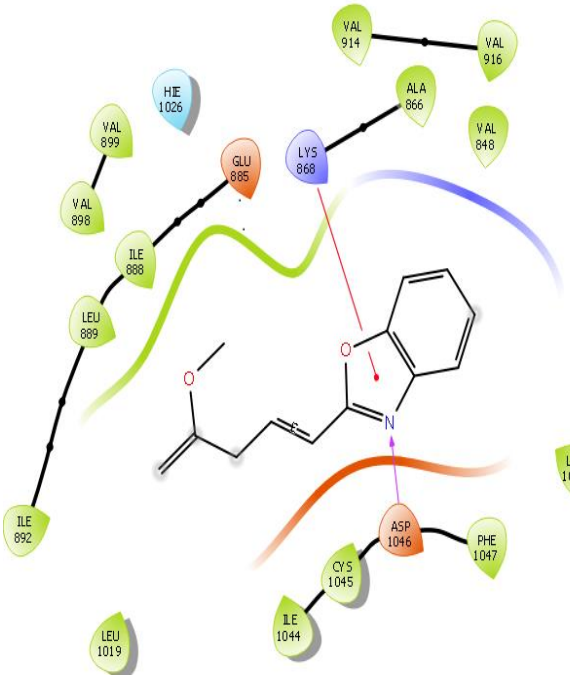
VAL 914
VAL 916
HIE 1026
ALA 866
VAL 899
VAL 848
GLU 885
LYS 868
VAL 898
ILE 888
LEU 889
ILE 892
ASP 1046
PHE 1047
CYS 1045
ILE 1044
LEU 1019

2(b)

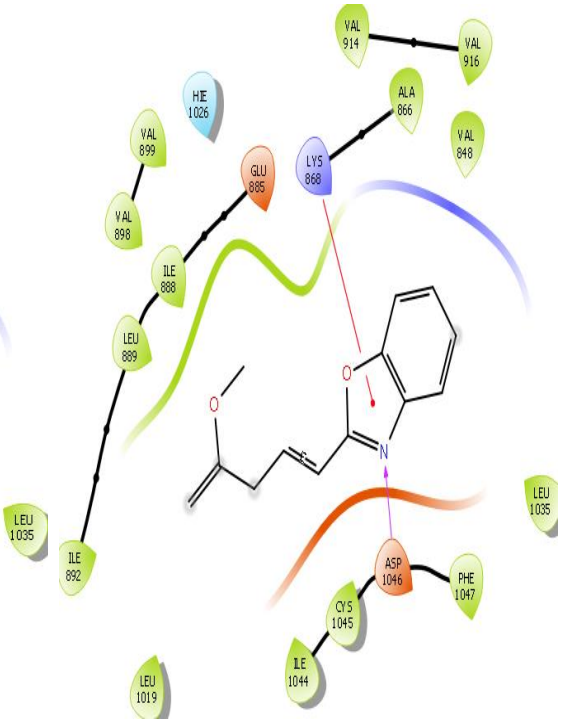
VAL 914
VAL 916
HIE 1026
ALA 866
VAL 899
VAL 848
GLU 885
LYS 868
VAL 898
ILE 888
LEU 889
LEU 1035
ILE 892
ASP 1046
PHE 1047
CYS 1045
ILE 1044
LEU 1019

(c)

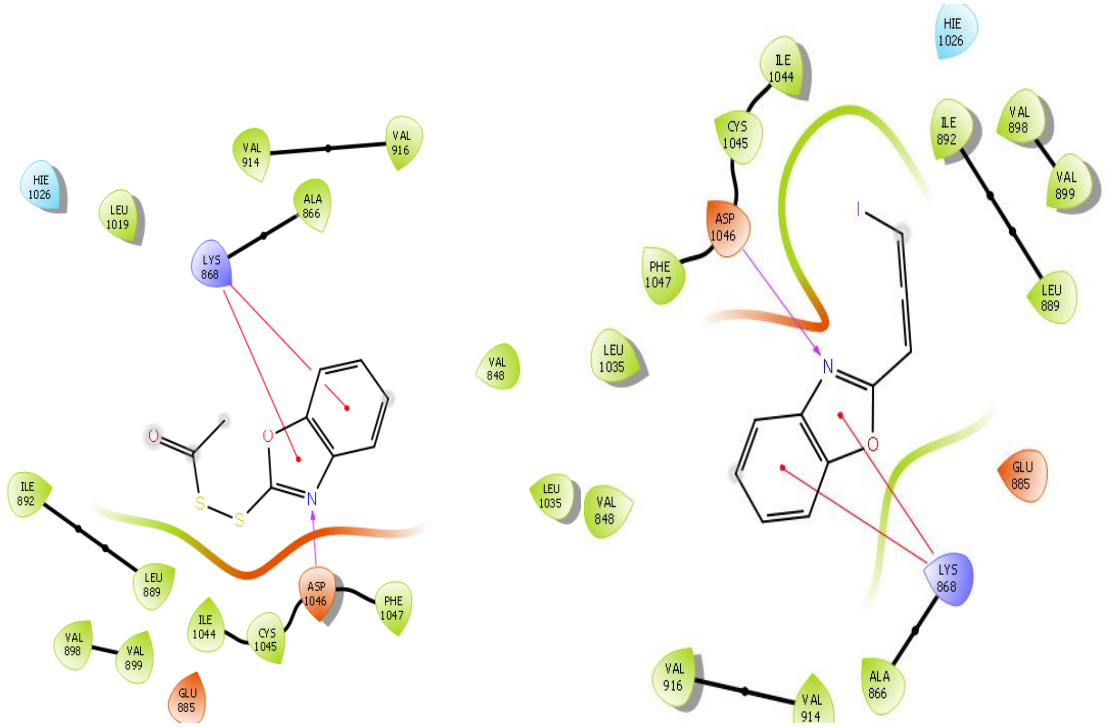

(d) **(e)**

Figure4.1.5: 1(a) 2D ligand interaction 1(b) 3D representation of binding orientation of the top-ranked compound CID170501037 .2D ligand interaction and surface binding of compound2 (b) CID142763609 (c) CID145008447 (d) CID88807689 (e) CID570281336..

Table4.1.3: XP docking results of the 5 topmost compounds against the protein VEGFR-2 (PDB ID: 1Y6A).

S. No.	Compounds	Chemical structure	Docking score(XP)
1	170501037	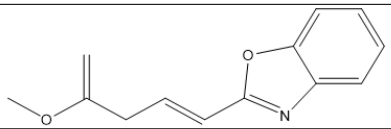	-9.12
2	142763609	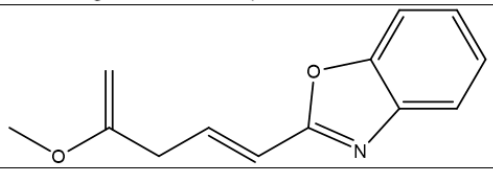	-8.71
3	145008447	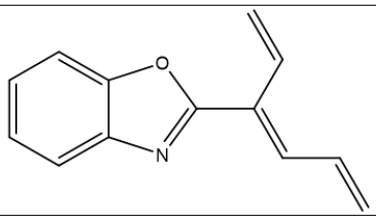	-8.67
4	88807689	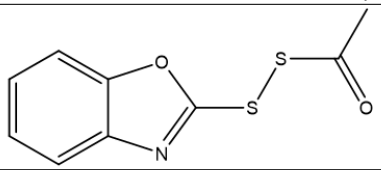	-8.65
5	57081336	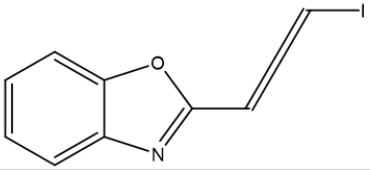	-8.63
6	Floxuridine	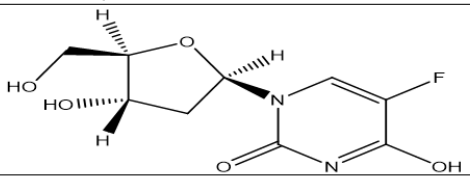	-7.87

Table 4.1.4: Ligand-Amino acid residues interactions and glide energy of the 5 topmost docked compounds.

S. no.	Ligand	Glide Energy (kcal/mol)	H-bond interactions	Amino acids residue
1.	170501037	-44.338	CYS 919, LYS 868(Br)	LYS868, ALA866, VAL916,GLU917, PHE918, CYS 919, LEU889, GLU885, CYS1045, ASP1046, PHE1047, PHE1047, GLY922, LEU840, LEU1035
2.	142763609	-40.519	CYS 1045	VAL898, HIE1026, ILE892, LEU889, ILE888, GLU885, LYS868, ALA866, ILE1044,CYS1045, ASP1046, PHE1047, LEU1035
3.	145008447	-33.249	CYS 1045	VAL899,ILE892,LEU889,GLU885,CYS1045,ILE1044,ASP1046,PHE1047, LYS868,VAL848
4.	88807699	-41.708	CYS 1045	ILE892, LEU889,ILE1044, CYS1045, ASP1046, PHE 1046,LYS868, ALA866
5.	57081336	-36.151	CYS 1045	LEU1035,PHE1047,ASP1046, CYS 1045, ILE 1044,VAL916, ALA866, LYS868, ILE892, LEU889, GLU885

4.1.5 ADME and toxicity profile prediction

The top five compounds identified through virtual screening were further evaluated for their pharmacokinetic and safety parameters using the ADMETlab 2.0 online platform. This step is essential to ensure drug-likeness and predict biological behavior within the human body. All selected molecules adhered to Lipinski's Rule of Five, confirming their potential as orally active drug candidates.

The ADME evaluation encompassed key physicochemical parameters, including molecular weight, lipophilicity (LogP), permeability across Caco-2 cell lines, and predicted human intestinal absorption (HIA). The LogP values of the shortlisted molecules fell within an optimal drug-like range of 2.093 to 3.588. Additionally, Caco-2 permeability scores were above −5.15 for all hits, indicating suitable membrane permeability. Blood-brain barrier penetration (logBB), volume of distribution (VD), and plasma protein binding (PPB) were also evaluated to forecast distribution and bioavailability.

Cytochrome P450 enzyme inhibition profiling revealed varying degrees of inhibitory potential for CYP1A2, CYP2C9, CYP2C19, CYP2D6, and CYP3A4—important metabolic enzymes for drug clearance. The compound CID 170501037 demonstrated favorable ADME properties with high predicted intestinal permeability, moderate CYP inhibition, and an acceptable clearance rate (Table 5.1.5).

For safety profiling, in silico toxicity tests were conducted to assess cardiotoxicity (hERG inhibition), mutagenicity (AMES test), skin sensitivity, and suitability for different routes of administration (ROA). Among the five compounds, CID 170501037 exhibited a very low hERG inhibition score (0.051) and was also non-mutagenic and skin-safe, indicating a strong safety margin and justifying its potential for further biological testing (Table 5.1.6).

comparative ADMET evaluation was conducted for the top five candidates using the ADMET Lab2.0 platform. All the molecules met the standard thresholds defined by Lipinski's Rule of Five, which includes criteria such as having no more than five hydrogen bond donors, no more than ten hydrogen bond acceptors, molecular weight below 500 Da, and LogP under 5. Additional properties, including brain penetration potential (logBB between 0.225 and −1.098), PPB, and VD, were also incorporated in the selection of the best lead compound (Table 5.1.5).

In silico toxicity studies were employed to evaluate the toxicity and adverse effects of the selected top 5 drug hits by utilizing the ADMET Lab2.0 online tool server which evaluated the results for.hERG blocker, Route of Administration, Skin senstivity and AMES Toxicity(Table5.1.6).

Table 4.1.5:Top 5 drug hits ADME predictions byADMET Lab 2.0

CID	**170501037**	**142763609**	**145008447**	**88807689**	**57081336**	**Excellent (green)**
Molecular weight	217.07	215.09	197.08	224.99	282.95	100-600
LogP	2.093	2.72	3.338	2.78	3.588	0 to3
Lipinski Rule	Accepted	Accepted	Accepted	Accepted	Accepted	
Caco-2 permeability	-4.537	-4.632	-4.764	-4.7	-4.625	>-5.15
HIA	0.005	0.004	0.006	0.007	0.004	0-0.3
BBB	0.978	0.892	0.437	0.229	0.769	
VD	01.538	0.626	0.617	0.352	1.374	0.04-20L
PPB	89.05%	92.02%	93.98%	94.54%	92.34%	≤90%
CYP1A2 inhibitor	0.99	0.993	0.9889	0.993	0.961	
CYP2C19 inhibitor	0.216	0.807	0.536	0.981	0.064	

CYP2C9 inhibitor	0.019	0.211	0.0342	0.93	0.048	0-1
CYP2D6 inhibitor	0.05	0.791	0.452	0.098	0.034	
CYP3A4 inhibitor	0.421	0.18	0.2	0.092	0.064	
CL	12.621	7.793	3.97	11.529	4.795	≥5

Table 4.1.6:Toxicity parameters of the top 5 drug hits by ADMET Lab 2.0

CID	hERG blocker	ROA	Skin sensitivity	AMES Toxicity
170501037	0.051	0.427	0.859	0.03
142763609	0.051	0.079	0.937	0.009
145008447	0.002	0.242	0.402	0.179
88807689	0.427	0.033	0.942	0.719
57081336	0.038	0.322	0.951	0.6

5.0 Summary

This research employed ligand-based computational modeling to evaluate benzoxazole derivatives for their potential as anticancer agents targeting VEGFR-2. A curated dataset of 93 compounds was subjected to pharmacophore modeling using the PHASE module, which identified a five-point hypothesis (AAHRR_1) featuring dual hydrogen bond acceptor sites, one hydrophobic interaction point, and two aromatic fragments critical features influencing biological activity.

Utilizing the AAHRR_1 hypothesis, a three-dimensional QSAR model was constructed and subjected to validation. The hypothesis demonstrated solid predictive strength, with statistical parameters such as $Q^2 = 0.7536$ and $R^2 = 0.8619$, along with an RMSE of 0.22, confirming its accuracy and reliability.

Virtual screening based on the model led to the retrieval of 595 structural analogs from the PubChem database. Molecular docking was carried out to determine their binding strength with VEGFR-2, revealing CID 170501037, the compound exhibited a docking energy of −9.116 kcal/mol, demonstrating stronger binding affinity than Floxuridine, which recorded an energy value of −7.865 kcal/mol. A stable hydrogen bond was established between the compound and the CYS919 residue of VEGFR-2, reflecting its improved binding efficiency.

The top five ligands were then analyzed for pharmacokinetic and toxicity profiles using ADMET Lab 2.0. Results showed that compounds like CID 170501037 and CID 145008447 had optimal drug-likeness and minimal toxicity, making them promising leads for further investigation. Overall, the study highlights these compounds as potential candidates for the development of VEGFR-2-targeted anticancer therapies, especially for treating colorectal cancer.

6 .0 REFERENCES

1. Raju, V. K. & Jha, A. New benzothiazole and benzoxazole picolinamide conjugates as potential anti-cancer agents: Design, synthesis, molecular docking and anticancer studies. J Mol Struct 1309, 138153 (2024).
2. Kakkar, S. et al. Design, synthesis and biological potential of heterocyclic benzoxazole scaffolds as promising antimicrobial and anticancer agents. Chem Cent J 12, 96 (2018).
3. Kuzu, B., Hepokur, C., Alagoz, M. A., Burmaoglu, S. & Algul, O. Synthesis, Biological Evaluation and In Silico Studies of Some 2-Substituted Benzoxazole Derivatives as Potential Anticancer Agents to Breast Cancer. ChemistrySelect 7, e202103559 (2022).
4. Tigga, P. et al. Examination of the synthetic processes for biologically strong benzoxazole derivatives. ~ 52 ~ Journal of Research in Chemistry 5, 52–63 (2024).
5. Philoppes, J. N. & Lamie, P. F. Design and synthesis of new benzoxazole/benzothiazole-phthalimide hybrids as antitumor-apoptotic agents. Bioorg Chem 89, 102978 (2019).
6. Raju, V. K. & Jha, A. New benzothiazole and benzoxazole picolinamide conjugates as potential anti-cancer agents: Design, synthesis, molecular docking and anticancer studies. J Mol Struct 1309, 138153 (2024).
7. Xiang, P. et al. Novel benzothiazole, benzimidazole and benzoxazole derivatives as potential antitumor agents: Synthesis and preliminary in Vitro biological evaluation. Molecules 17, 873–883 (2012).
8. Kumar M, Ramasamy K, Mani V, Mishra RK, Majeed ABA, De Clercq E, et al. Synthesis, antimicrobial, anticancer, antiviral evaluation and QSAR studies of 4-(1-aryl-2-oxo-1, 2-dihydro-indol-3-ylideneamino)-N-substituted benzene sulfonamides. Arabian Journal of Chemistry. 2014;7(4):396-408.
9. J. Osipiuk JH, R. Jedrzejczak, E. Rubin , K. Guinn, D. Ioerger, T. Baker, J. Sacchettini, A. Joachimiak. Thymidylate synthase from Staphylococcus aureus. 2012.

10. Friesner RA, Banks JL, Murphy RB, Halgren TA, Klicic JJ, Mainz DT, et al. Glide: a new approach for rapid, accurate docking and scoring. 1. Method and assessment of docking accuracy. Journal of medicinal chemistry. 2004;47(7):1739-49.

11. . R.A. Friesner JLB, R.B. Murphy, T.A. Halgren, J.J. Klicic, D.T. Mainz, M.P. Repasky, E. H. Knoll, M. Shelley, J.K. Perry, and D.E. Shaw, . Glide: A new approach for rapid, accurate docking and scoring. Method and assessment of docking accuracy,. J Med Chem. 2004;47: 1739–49.

12. Madhavi Sastry G, Adzhigirey M, Day T, Annabhimoju R, Sherman W. Protein and ligand preparation: parameters, protocols, and influence on virtual screening enrichments. Journal of computer-aided molecular design. 2013;27(3):221-34.

13. Tyagi R, Singh A, Chaudhary KK, Yadav MK. Chapter 17 - Pharmacophore modeling and its applications. In: Singh DB, Pathak RK, editors. Bioinformatics: Academic Press; 2022. p. 269-89.

14. Dixon SL, Smondyrev AM, Rao SN. PHASE: A Novel Approach to Pharmacophore Modeling and 3D Database Searching. 2006;67(5):370-2.

15. Pai P, Kumar A, Shetty MG, Kini SG, Krishna MB, Satyamoorthy K, et al. Identification of potent HDAC 2 inhibitors using E-pharmacophore modelling, structure-based virtual screening and molecular dynamic simulation. 2022;28(5):119.

16. Mali S, Chaudhari H. Molecular modelling studies on adamantane-based Ebola virus GP-1 inhibitors using docking, pharmacophore and 3D-QSAR. SAR and QSAR in Environmental Research. 2019;30(3):161-80.

17. Arisoy M, Temiz-Arpaci O, Yildiz I, Kaynak-Onurdag F, Aki E, Yalcin I, et al. Synthesis, antimicrobial activity and QSAR studies of 2,5-disubstituted benzoxazoles. SAR and QSAR in Environmental Research. 2008;19(5-6):589-612.

18. Sanapalli BKR, Yele V, Baldaniya L, Karri VVSR. Identification of novel protein kinase C-βII inhibitors: virtual screening, molecular docking and molecular dynamics simulation studies. Journal of Molecular Modeling. 2022;28(5):117.

19. Kashid BB, Ghanwat AA, Khedkar VM, Dongare BB, Shaikh MH, Deshpande PP, et al. Design, Synthesis, In Vitro Antimicrobial, Antioxidant Evaluation, and Molecular Docking Study of Novel Benzimidazole and Benzoxazole Derivatives. Journal of heterocyclic chemistry. 2019;56(3):895-908.

20. Opo FADM, Rahman MM, Ahammad F, Ahmed I, Bhuiyan MA, Asiri AM. Structure based pharmacophore modeling, virtual screening, molecular docking and ADMET approaches for identification of natural anti-cancer agents targeting XIAP protein. Scientific reports. 2021;11(1):4049.

21. Rezazadeh M, Pordel M, Davoodnia A, Saberi S. New fluorescent 3H-imidazo[4,5-e][2,1]benzoxazoles: synthesis, spectroscopic characterization, and antibacterial activity. Chemistry of Heterocyclic Compounds. 2015;51(10):918-22.

22. Gupta S, Baweja GS, Singh S, Irani M, Singh R, Asati VJEJoMC. Integrated fragment-based drug design and virtual screening techniques for exploring the antidiabetic potential of thiazolidine-2, 4-diones: Design, synthesis and in vivo studies. 2023;261:115826.

23. Ertan-Bolelli T, Yildiz İ, Ozgen-Ozgacar S. Synthesis, molecular docking and antimicrobial evaluation of novel benzoxazole derivatives. Medicinal Chemistry Research. 2016;25(4):553-67.

24. Manal M, Manish K, Sanal D, Selvaraj A, Devadasan V, Chandrasekar MJN. Novel HDAC8 inhibitors: A multi-computational approach. SAR and QSAR in Environmental Research. 2017;28(9):707-33.

25. Golbraikh A, Tropsha A. Predictive QSAR modeling based on diversity sampling of experimental datasets for the training and test set selection. Molecular Diversity. 2000;5(4):231-43.